IEEE Open Journal of
Antennas and Propagation

Received 3 August 2023; revised 11 September 2023; accepted 22 September 2023. Date of publication 26 September 2023;
date of current version 13 October 2023.

Digital Object Identifier 10.1109/OJAP.2023.3319533

Excitation Diversity in Adaptively Thinned Arrays for Microwave Sensing Applications

SANDRA COSTANZO [1,2,3,4] (Senior Member, IEEE), AND GIOVANNI BUONANNO [1,2] (Member, IEEE)

[1]DIMES, University of Calabria, 87036 Rende, Italy

[2]Inter-University National Research Center on Interactions Between Electromagnetic Fields and Biosystems, 16145 Genoa, Italy

[3]Consorzio Nazionale Interuniversitario per le Telecomunicazioni, 43124 Parma, Italy

[4]National Research Council, Institute for Electromagnetic Sensing of the Environment, 80124 Naples, Italy

CORRESPONDING AUTHOR: G. BUONANNO (e-mail: giovanni.buonanno@unical.it)

This work was supported by the Ministero dell'Università e della Ricerca (MUR), Italy, as part of Italian National Project PON ARS01_00536 "OCEANOS," and as part of "Programma Operativo Nazionale Ricerca e Innovazione 2014–2020" (PON "Ricerca e Innovazione" 2014–2020) Project "Non-Invasive Electromagnetic Green Devices and Methods for Advanced Medical Diagnostics."

ABSTRACT Thinned arrays are a class of non-uniform arrays in which the magnitudes of the excitation coefficients usually take on binary values. They are obtained by removing or connecting to matched loads the elements of a filled array, such that the final combination of active elements resembles that of a reference unequally-excited filled array. However, the advantage of reducing the complexity of the feeding network can lead, in some applications (such as in microwave sensing), to an unacceptable discrepancy between the actual radiation pattern and the desired one, especially for small to medium-sized arrays. In this work, an excitation diversity technique is included in thinned arrays design to overcome the above drawback. Data distributions achieved with the above approach are averaged to obtain potential high-quality final images. Moreover, the proposed methodology can be easily implemented in real-time adaptive arrays. The reported numerical results successfully prove the suitability of the proposed diversity technique, to be usefully applied for microwave sensing applications.

INDEX TERMS Adaptive arrays, diversity techniques, microwave sensing, thinned arrays.

I. INTRODUCTION

THINNED arrays are non-uniform arrays obtained by removing (first option) or deactivating (second option) radiators from a filled periodic reference array [1]. Essentially, the magnitudes of the excitation coefficients are represented by binary variables. The first option saves a different number of antennas and associated T/R modules. Furthermore, since the shaping of the radiation pattern is performed through the same thinning procedure, the amplifiers of the feeding network can all operate at the maximum power [2], [3], [4], [5]. Such types of thinned arrays can be exploited for all those applications where high resolution is strongly required, but not necessarily related to high gain, such as, for example, in satellite applications, ground-based high-frequency radars, or radio astronomy [6]. It is worth highlighting that thinned array methodology can also be applied to reflectarray antennas [7], [8]. The second option provides final arrays that are still filled, as the inactive antenna elements are not removed but connected to matched loads. Consequently, mutual couplings can be more controllable, as the periodic array lattice is not subject to perturbations [1]. However, it is worth mentioning that several methods can be used to reduce the undesired effect of mutual couplings [9], [10], [11], [12], [13].

Several stochastic optimisation algorithms have been developed for the synthesis of thinned arrays [14], [15], [16], [17], [18], to be suitable for arrays of arbitrary size. However, these methods may require a high computational cost for large arrays [19]. Dynamic programming has been also exploited in thinned arrays [20]. While this methodology has proven successful even for large arrays, the optimal solution is not always guaranteed. Approaches based on the Fourier-based iterative technique [21], [22], [23], exploiting the link between the excitation coefficients and the array factor, should be also mentioned. These techniques may require a lower computational burden as compared to

stochastic optimisation algorithms. However, they are based on an iterative procedure and require the heuristic choice of a threshold to decide which radiators should be turned-on.

The methodologies mentioned above can be effective for the design of thinned arrays. However, they do not allow for an easy *a priori* analysis of the array performance, and, in general, they are not suitable for real-time systems. For this reason, the oldest design methodology of statistical thinning [24], [25] has been re-evaluated in recent years. This methodology has proved to be effective for implementing dynamic and adaptive arrays [19], [26], [27]. In fact, it is a simple and fast procedure [26], and it is also more complete from an analytical point of view, as compared to other approaches.

To the best of the authors' knowledge, statistical thinning dates back to the 1960s. It is worth noting that its actual definition was introduced in [25], where the spatial density of radiators is statistically proportional to the real and positive reference current. In particular, the magnitudes of the excitation coefficients are modelled as binary random variables, whose mean coincides with the magnitudes of the excitation coefficients of the reference filled array. Consequently, the array factor is a stochastic process. In [28], at the expense of an increased complexity in the feeding network, more than two levels are considered for the magnitudes of the excitation coefficients. In this context, the analysis of statistically thinned arrays based on the theory of random arrays is worth mentioning [29], [30]. Indeed, for statistically thinned arrays, probabilistic analysis approaches similar to those recently proposed in the literature can be adopted [5], [31], [32], [33], [34], [35], [36]. In the context of statistical thinning, methodologies for synthesising multi-beam [39] and broadband [40] thinned arrays have been also introduced recently. In particular, the thinned arrays proposed in [40] can exploit broadband techniques for integrating different technologies [41]. It is also worth highlighting that the analysis methodologies developed for (far-field) statistically thinned arrays have recently been further developed in the framework of the tolerance theory of near-field focused antenna arrays [42].

Statistically thinned arrays can suffer from high sidelobes level even when composed of a large number of elements, as shown in [25]. In fact, each different combination of excitation coefficients provides a different pattern. A simple solution may be to generate a certain number of such combinations and to find the realisation (sample path) of the array factor closest to the reference one. The choice of the number of combinations could be based on recent arguments on the distance characterisation concerning the actual pattern and the desired one [29], [39]. However, there can be a considerable number of array factor realisations, and the best one is not sure to match the design specifications.

To overcome the above significant drawback, array systems based on statistical thinning are proposed in this work which exploit a particular diversity technique to obtain patterns with higher performance in terms of lower levels for the peak sidelobe-level, and smaller discrepancy with respect to the desired pattern. These arrays are more appropriate for working in receiving mode. Therefore, the context of microwave sensing is the most suitable for exploiting the potential of this type of thinned arrays. The applied diversity technique, hereinafter referred as *excitation diversity*, is inspired by the methodology presented in [43]. However, instead of position or frequency diversity, different combinations of magnitudes of the excitation coefficients are considered to which different structures of the acquired (complex) potential data are associated. A sample mean is then performed on these data to improve the final quality of the sensing process. It is worth highlighting that, as compared to [43], the implementation of the excitation diversity in thinned arrays is less complex, as it does not require broadband or frequency hopping-based generators, nor moving the radiators before making each acquisition. Instead, the signal coming from fixed elements is only required to pass or not inside the feeding network, working at a single frequency. This can be done by inserting proper switches to provide for the possible closing on matched loads of signals coming from the elements to be turned off, depending on the particular combination of the excitation coefficients which are implemented in the generic sensing acquisition. It is worth pointing out that the use of the described diversity technique not only allows for a decrease in the distance between the actual pattern and the desired one, but, as with any (temporal, frequency, spatial, *et cetera*) diversity technique [44], it could also reduce fading and noise. However, the proposed methodology is specifically designed for systems based on thinned arrays. Moreover, due to the statistical thinning, the proposed system can be quickly reconfigured by changing the random seed of the array excitation coefficient generator. Furthermore, its structure is suitable for easily implementing adaptive algorithms. In this way, it could be seen as a possible evolution of systems presented in [26], [27]. It is also worth pointing out that statistical thinning schemes could be devised which exploit the excitation diversity in transmission mode. These could perform multiple transmissions towards the receiving system, each associated with a different combination of the excitation coefficients, which could then implement the averaging operations.

The remainder of the paper is organized as follows: Section II describes the model of the reference filled array; in Section III, the fundamental principles of statistical thinning are recalled; in Section IV, statistically thinned arrays exploiting excitation diversity are presented; Section V shows some significant numerical results; finally, the conclusions are outlined in Section VI. The discussed numerical results validate the illustrated theoretical concepts, thus confirming the potential application of the proposed approach in the framework of microwave sensing. The paper also includes two appendices: Appendix A reports the nomenclature of the most important quantities, while Appendix B reports detailed computations which are omitted in the main text.

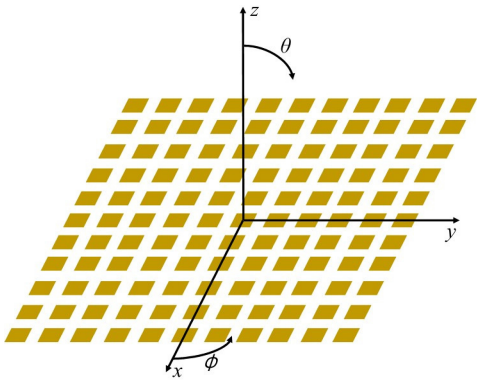

FIGURE 1. Representation of a generic filled periodic array together with the observation angles.

II. REFERENCE ARRAY MODEL

Let us consider N similar sensors immersed into a free-space-like medium, and arranged in the $x-y$ plane of an orthogonal Cartesian reference system and having the same orientation (see Fig. 1). Assume that mutual couplings between adjacent elements are negligible, as well as the so-called spatially correlated and random errors [6]. In this case, the far field is proportional to the following complex array factor [1]:

$$F_{ref}(u,v) = \sum_{n=1}^{N} A_n \, e^{j2\pi(x_n u + y_n v)} \tag{1}$$

where $\{A_n\}_{n=1}^{N}$ are real and positive excitation coefficients realizing the amplitude tapering; (x_n, y_n) is the position of n-th sensor, expressed in wavelengths; $u = \sin\theta\cos\phi - \sin\theta_0\cos\phi_0 \in [-2, 2]$ and $v = \sin\theta\sin\phi - \sin\theta_0\sin\phi_0 \in [-2, 2]$, with $\theta \in [0, \pi]$ and $\phi \in [0, 2\pi]$ being the zenithal and azimuthal observation angles, respectively, and (θ_0, ϕ_0) the *steering direction*. In this case, the so-called *full scan-range* coincides with the circularly-bounded domain centred at $(u, v) = 0$ and having radius equal to 2 [40]. The model given by eq. (1) is related to arrays whose radiation pattern has only one main lobe and several secondary lobes. The position of the main lobe maximum is controlled by means of the steering angles θ_0 and ϕ_0, to which suitable phase-shifters are associated. Furthermore, the spacing between the radiators must be such as not to let the so-called grating lobes enter the visible space.

The reference array elements are arranged in a rectangular grid and equally spaced along x and y by half a wavelength. The coordinates of the sensor locations are as follows:

$$\begin{aligned} x_n &= -\frac{L_x}{2} + (n-1)\frac{L_x}{N_x - 1} \qquad n = 1, 2, \ldots, N_x \\ y_n &= -\frac{L_y}{2} + (n-1)\frac{L_y}{N_y - 1} \qquad n = 1, 2, \ldots, N_y \end{aligned} \tag{2}$$

where $N_x \times N_y = N$, *i.e.*, the total number of elements is given by the product of the number of elements arranged parallel to the x-axis with the number of elements arranged parallel to the y-axis. The parameters L_x and L_y represent the dimensions (in wavelengths) of the array aperture along x and y, respectively. Since the spacing between the elements must equal half a wavelength, $L_x/(N_x-1) = 0.5$ and $L_y/(N_y-1) = 0.5$. Also, for simplicity, it is assumed that $N_x = N_y$ and $L_x = L_y$.

III. CLASSIC ARRAY THINNING

Referring to the array factor given by eq. (1), the classic statistical thinning procedure consists in considering the following function [29]:

$$F(u,v) = C \sum_{n=1}^{N} F_n \, e^{j2\pi(x_n u + y_n v)} \tag{3}$$

where $\{F_n\}_{n=1}^{N}$ are binary (Bernoulli) random variables such that $\mathcal{P}_r\{F_n = 1\} = 1 - \mathcal{P}_r\{F_n = 0\} = E[F_n] = p_n = \alpha\,(A_n/\max\{A_n\}_{n=1}^{N})$, with $\mathcal{P}_r\{\cdot\}$ and $E[\,\cdot\,]$ being the probability measure and the expected value operator, respectively; $C = \max\{A_n\}_{n=1}^{N}/\alpha$; $0 < \alpha \leq 1$ is the *thinning factor*. From Eq. (3), the array factors of thinned arrays can be derived. Indeed, since $\{F_n\}_{n=1}^{N}$ are random coefficients, $F(u, v)$ is a stochastic process to be analyzed by means of probability theory. A generic thinned array is obtained from this function by generating one of several combinations of the coefficients $\{F_n\}_{n=1}^{N}$. Therefore, a generic thinned array configuration corresponds to a realisation (sample path) of $F(u, v)$.

The mean (expected value) of $F(u, v)$ is given as follows:

$$\begin{aligned} \mu(u,v) &= E[F(u,v)] = C \sum_{n=1}^{N} E[F_n] \, e^{j2\pi(x_n u + y_n v)} \\ &= \frac{\max\{A_n\}_{n=1}^{N}}{\alpha} \sum_{n=1}^{N} \frac{\alpha\, A_n}{\max\{A_n\}_{n=1}^{N}} \, e^{j2\pi(x_n u + y_n v)} \\ &= \sum_{n=1}^{N} A_n \, e^{j2\pi(x_n u + y_n v)} \end{aligned} \tag{4}$$

It represents the array factor, $\mu(u, v) = F_{ref}(u, v)$, of the reference filled array. Referring to the squared magnitude of $F_{ref}(u, v)$ (see the Appendix), the mean of the power-pattern, $P(u, v) = |F(u, v)|^2$, can be written as:

$$\begin{aligned} \mu_P(u,v) &= E[P(u,v)] \\ &= C^2 \sum_{n=1}^{N}\sum_{m=1}^{N} E[F_n F_m] e^{j2\pi[(x_n - x_m)u + (y_n - y_m)v]} \\ &= C^2 \sum_{n=1}^{N} E\left[F_n^2\right] + C^2 \sum_{n=1}^{N}\sum_{m=1, m\neq n}^{N} \Big\{ E[F_n]E[F_m] \\ &\qquad \times e^{j2\pi[(x_n - x_m)u + (y_n - y_m)v]} \Big\} \\ &= \sum_{n=1}^{N} \frac{A_n \max\{A_n\}_{n=1}^{N}}{\alpha} + \sum_{n=1}^{N}\sum_{m=1, m\neq n}^{N} \Big\{ A_n A_m \\ &\qquad \times e^{j2\pi[(x_n - x_m)u + (y_n - y_m)v]} \Big\} \\ &= \left|F_{ref}(u,v)\right|^2 + \sum_{n=1}^{N} \left(\frac{A_n \max\{A_n\}_{n=1}^{N}}{\alpha} - A_n^2 \right) \end{aligned} \tag{5}$$

where, in the last line of eq. (5), the term added to $|F_{ref}(u,v)|^2$ represents the variance of the array factor, namely, $\sigma^2 = \sum_{n=1}^{N} [A_n (\max\{A_n\}_{n=1}^{N}/\alpha) - A_n^2]$ (note that the variance is constant).

The statistical structure underlying the generation of coefficients $\{F_n\}_{n=1}^{N}$ is so that a spatial tapering can be obtained, which emulates the amplitude tapering of the reference unequally-excited periodic array. Therefore, the elements of the thinned array are more concentrated where the reference amplitude tapering assumes higher levels. However, in practice, the classic statistical thinning allows to obtain a non-uniform array configuration related to a single realisation of the aforementioned binary coefficients. This implies that the discrepancy between the actual radiation pattern and the reference one can be considerable. It is worth highlighting the difference between the predicted average side-lobe levels and the actual ones reported in [25], with the latter having values approximately 8 dB higher than the former. For this reason, in the following, a methodology is proposed for thinned arrays that can be used in the context of microwave sensing so to limit the aforementioned discrepancy.

IV. THINNED ARRAYS OF SENSORS WITH INCORPORATED EXCITATION DIVERSITY

The thinning operation implies some kind of degradation in the radiation diagram, such as, for example, an increase in the side lobes levels with respect to the reference diagram [29], [40]. This, of course, has more impact in the case of small and medium-sized thinned arrays. As shown in [43], diversity techniques can help counteract the above disadvantages. However, unlike [43], the excitation diversity is exploited here, adapting a methodology presented in [26] to the microwave sensing problem. Thus, the imaging system under consideration owns the following features:

1) The thinning operation performs amplitude tapering. As above, the excitation coefficients are modelled in terms of binary random variables. These are used to carry out a less expensive amplitude tapering in terms of feeding network complexity, as compared to the standard amplitude tapering, where different amplifiers are adopted for each excitation coefficient. Instead, the proposed system may include a single power amplifier and, subsequently, a single analogue-to-digital converter to process the acquired data adequately.
2) The system could be designed to work both in receiving mode and in transmitting/receiving mode. In receiving-only arrays, modified T/R modules can be used which include only the receiving chain, while the switch output usually connected to the transmitting chain is closed on a matched load.
3) In transmitting/receiving arrays, each array element can be associated with a T/R module, such as that described in [26], where an absorptive single-pole triple throw (SP3T) switch is included. This leads to select both the transmission and the receiving paths, as well as to realize the connection with a matched load, so to have no reflections, and lead the relative array element to be inactive. The switching time can be assumed equal to 1 μs, corresponding to high-performance switches. Furthermore, it is possible to exploit SP3T switches which have an insertion loss greater than -1.3 dB in the $[0, 6]$ GHz frequency band [45].
4) The system performs multiple *independent* acquisitions, each one associated with a different independent combination of the excitation coefficients $\{F_n\}_{n=1}^{N}$. These are associated with different field distributions, which are averaged to obtain an array factor similar to that of a reference filled amplitude-tapered array.
5) Since the statistical thinning procedure turns out to be extremely fast, the proposed system can be made easily reconfigurable and working in real-time. Lookup tables can be implemented and consulted which contain the excitation coefficients associated with the desired configurations of the array factor.
6) To implement an adaptive system, and therefore to take also into account those phenomena that can distort the array factor, such as mutual coupling effects, specific near-field to far-field transformation techniques [46] can be exploited in such a way to have a feedback and dynamically control, similarly to [26], the realisations of the random excitation coefficients.
7) The proposed system can also provide multiple acquisition chains, each one associated with an independent array factor, in a conceptual way as similar to scheme 1 presented by the authors in [39]. In particular, being N the number of antenna elements and M the number of independent array factors, M independent space observations can be obtained.
8) It is worth emphasizing that, regardless of the type of array used (thinned or not), taking advantage of multiple acquisitions also allows for noise and fading reduction.

In light of the above considerations, the proposed system can be seen as an *adaptively thinned array incorporating excitation diversity*.

At this point, let us introduce the excitation diversity paradigm. It consists of the following descriptive points:

- The system acquires Q realisations (sample paths) of the thinned array factor, and their average is subsequently performed. From a conceptual point of view, it is equivalent to the situation where Q independent statistically thinned arrays, having the same geometric and statistical characteristics, are considered, and the realisations of their array factors are averaged.
- At the initial time, the set of order $q = 1$ of $\{F_n\}_{n=1}^{N}$ is considered, *i.e.*, $\{F_n^{(1)}\}_{n=1}^{N}$, which is associated with the first statistically thinned array. Thus, the current (random) array output depends on the following array

factor:

$$F_1(u,v) = C\sum_{n=1}^{N} F_n^{(1)}\, e^{j2\pi(x_n u + y_n v)} \tag{6}$$

The realisations of $\{F_n^{(1)}\}_{n=1}^N$ gives a particular sample path for $F_1(u,v)$, which in turn is associated with a particular realisation of the array output to be digitised and stored.

- Subsequently, the set of order 2 of random variables $\{F_n\}_{n=1}^N$ is considered, that is, $\{F_n^{(2)}\}_{n=1}^N$, which is **independent** on the set of order 1. However, it is worth noting that although the set $\{F_n^{(1)}\}_{n=1}^N$ and $\{F_n^{(2)}\}_{n=1}^N$ are statistically independent, the generic coefficients $F_n^{(1)}$ and $F_n^{(2)}$ are identically distributed. The switches are re-set based on the new values assumed by the realisations of $\{F_n^{(2)}\}_{n=1}^N$. Therefore, a new random array factor must be considered:

$$F_2(u,v) = C\sum_{n=1}^{N} F_n^{(2)}\, e^{j2\pi(x_n u + y_n v)} \tag{7}$$

A given sample path of $F_2(u,v)$ provides a relative realisation of the array output. In this case, the current array output is digitised, added to the array output from the previous point, and the result is stored. So, it is equivalent to the situation where the random function $F_1(u,v) + F_2(u,v)$ is considered, whose particular sample path is associated with a particular realisation of the equivalent array output.

- By repeating several times the previous operations, the following sample mean of Q independent random array factors can be considered, namely:

$$\begin{aligned} F_{ed}(u,v) &= \frac{1}{Q}\sum_{q=1}^{Q} F_q(u,v) \\ &= C\sum_{n=1}^{N}\left[\frac{1}{Q}\sum_{q=1}^{Q} F_n^{(q)}\right] e^{j2\pi(x_n u + y_n v)} \\ &= C\sum_{n=1}^{N} F_{n_{ed}}\, e^{j2\pi(x_n u + y_n v)} \end{aligned} \tag{8}$$

where the subscript *ed* stands for *excitation diversity*, taking into account that $F_q(u,v)$ is the array factor of the thinned array associated with the set of order q of the binary random variables $\{F_n^{(q)}\}_{n=1}^N$. The function $F_{ed}(u,v)$ can be seen as the (equivalent) actual array factor approximating the reference one with greater accuracy as compared to $F(u,v)$ given by eq. (3). Indeed, this can be demonstrated by considering both the mean and the mean squared magnitude of $F_{ed}(u,v)$.

Accordingly to the above argumentations, and referring to the Appendix for the characterisation of the individual $F_q(u,v)$, the mean of $F_{ed}(u,v)$ is given as:

$$\begin{aligned} \mu_{ed}(u,v) &= E[F_{ed}(u,v)] \\ &= \frac{1}{Q}\sum_{q=1}^{Q} E\big[F_q(u,v)\big] \\ &= \mu(u,v) = F_{ref}(u,v) \end{aligned} \tag{9}$$

while the mean of $P_{ed}(u,v) = |F_{ed}(u,v)|^2$ is given by the following expression:

$$\begin{aligned} E[P_{ed}(u,v)] &= E\Big[|F_{ed}(u,v)|^2\Big] \\ &= E\left[\frac{1}{Q^2}\sum_{q=1}^{Q}\sum_{h=1}^{Q} F_q(u,v)F_h^*(u,v)\right] \\ &= \frac{1}{Q^2}\sum_{q=1}^{Q} E\Big[|F_q(u,v)|^2\Big] \\ &\quad + \frac{1}{Q^2}\sum_{q=1}^{Q}\sum_{h=1,h\neq q}^{Q} E\big[F_q(u,v)\big]E\big[F_h^*(u,v)\big] \\ &= \frac{1}{Q^2}\sum_{q=1}^{Q}\mu_P(u,v) + \frac{1}{Q^2}\sum_{q=1}^{Q}\sum_{h=1,h\neq q}^{Q}|\mu(u,v)|^2 \\ &= \frac{|\mu(u,v)|^2 + \sigma^2}{Q} + \left(1-\frac{1}{Q}\right)|\mu(u,v)|^2 \\ &= |\mu(u,v)|^2 + \frac{\sigma^2}{Q} \\ &= \big|F_{ref}(u,v)\big|^2 + \frac{\sigma^2}{Q} \end{aligned} \tag{10}$$

thus obtaining a lower dispersion with respect to the case in which the excitation diversity is absent. The term σ^2/Q represents the variance of $F_{ed}(u,v)$. Thus, by changing the number of acquisitions, it is possible to easily control the statistical dispersion of $F_{ed}(u,v)$.

A. CONCEPTUAL ASPECTS OF THE PROPOSED DIVERSITY TECHNIQUE

The proposed technique is based on the *(weak) law of large numbers*. In particular, by Markov's theorem [48], the following *sample mean* associated with the sequence of independent and identically distributed (*i.i.d*) real random variables $Z_1, Z_2, \ldots, Z_Q, \ldots,$:

$$\overline{Z} = \frac{1}{Q}\sum_{q=1}^{Q} Z_q \tag{11}$$

satisfies the following relationship:

$$\lim_{Q\to\infty} \mathcal{P}_r\big\{\big|\overline{Z} - \mu_Z\big| \leq \gamma\big\} = 1 \tag{12}$$

if $\sigma_Z^2 \to 0$ as $Q \to \infty$, with μ_Z and $Q \times \sigma_Z^2$ being the common expected value and variance of the above *i.i.d.* random variables and γ any positive constant. Consequently, since γ can be made as small as desired, the sample mean can be arbitrarily close to μ_Z for sufficiently high values

of Q. Of course, in the case of complex random variables, it is possible to operate on the real and imaginary parts.

The above argument can represent a justification for the presented methodology. Indeed, the proposed technique can be regarded as an implementation of the law of large numbers, recognising that $F_{ed}(u,v)$ is the sample mean of Q *i.i.d.* thinned array factors. For the sake of clarity, let us rewrite the array factor, given by Eq. (8), as follows:

$$\begin{aligned} F_{ed}(u,v) &= F_{ed_{\mathcal{R}}}(u,v) + jF_{ed_{\mathcal{I}}}(u,v) \\ &= \frac{1}{Q}\sum_{q=1}^{Q} F_{q_{\mathcal{R}}}(u,v) + j\frac{1}{Q}\sum_{q=1}^{Q} F_{q_{\mathcal{I}}}(u,v) \end{aligned} \quad (13)$$

where $F_{ed_{\mathcal{R}}}(u,v)$ and $F_{ed_{\mathcal{I}}}(u,v)$ are the real and the imaginary parts of $F_{ed}(u,v)$, respectively, while $F_{q_{\mathcal{R}}}(u,v)$ and $F_{q_{\mathcal{I}}}(u,v)$ represent the real and the imaginary parts of $F_q(u,v)$, respectively. It is worth remembering (see Eq. (9)) that, for each q, the expected value of $F_{q_{\mathcal{R}}}(u,v)$ is equal to the real part of $F_{ref}(u,v)$, while the expected value of $F_{q_{\mathcal{I}}}(u,v)$ is equal to the imaginary part of $F_{ref}(u,v)$. Considering the real part of $F_{ed}(u,v)$, it can be seen that, at the generic point (u,v), the quantities $F_{1_{\mathcal{R}}}(u,v)$, $F_{2_{\mathcal{R}}}(u,v),\ldots,$ $F_{Q_{\mathcal{R}}}(u,v)$ are *i.i.d* real random variables, since the sets of binary random coefficients $\{F_n^{(1)}\}_{n=1}^N$, $\{F_n^{(2)}\}_{n=1}^N,\ldots,$ $\{F_n^{(Q)}\}_{n=1}^N$ associated with them are independent and identically distributed, *i.e.*, $F_n^{(1)}, F_n^{(2)},\ldots, F_n^{(Q)}$ are *i.i.d.* binary random variables, for each n. Consequently, as stated above, observing that $\sigma^2_{\mathcal{R}}(u,v)$ becomes increasingly smaller as Q increases, with $Q\times\sigma^2_{\mathcal{R}}(u,v)$ being the common variance of $F_{1_{\mathcal{R}}}(u,v)$, $F_{2_{\mathcal{R}}}(u,v),\ldots,$ $F_{Q_{\mathcal{R}}}(u,v)$ (see Appendix B), it can be said that the statistical dispersion of $F_{ed_{\mathcal{R}}}(u,v)$ around the real part of $F_{ref}(u,v)$ becomes increasingly smaller as Q increases. The same argument can be made for the imaginary part of $F_{ed}(u,v)$, considering the term $\sigma^2_{\mathcal{I}}(u,v)$, with $Q\times\sigma^2_{\mathcal{I}}(u,v)$ being the common variance of $F_{1_{\mathcal{I}}}(u,v)$, $F_{2_{\mathcal{I}}}(u,v),\ldots,$ $F_{Q_{\mathcal{I}}}(u,v)$ (see Appendix B). Therefore, it can be derived that, as Q increases, the realisations of $F_{ed}(u,v)$ are increasingly closer to $F_{ref}(u,v)$, taking into account that, by means of Eq.(25) and Eq.(26), $\sigma^2/Q = [\sigma^2_{\mathcal{R}}(u,v)+\sigma^2_{\mathcal{I}}(u,v)]$. From a practical point of view, the proposed system implements the rule of the arithmetic mean employed in the theory of measurements [48]. Indeed, in this framework, $F_{ref}(u,v)$ can be seen as the quantity for which an estimate may be obtained, and achieved precisely from the arithmetic mean of the quantities $\{F_q(u,v)\}_{q=1}^Q$ representing independent measurements which are performed in almost identical conditions. Consequently, the algorithm implemented by the proposed system is not intended to completely eliminate the discrepancy between the actual and the desired array factors, requiring an infinite number of acquisitions, but rather to control such discrepancy in a sufficiently flexible way by acting on the number of acquisitions.

B. COMPLEXITY ESTIMATION

The architecture of the proposed system can be of the *corporate feed* type [1], in which an analog beamforming is first performed, and the total signal, coming from the combination of the signals given by each sensor, is converted into a digital form by using a single analog-to-digital converter (*ADC*). Therefore, from the beamforming point of view, the proposed system has the same complexity as a conventional thinned phased array, except that the T/R modules are required also to provide the possibility of connection to a matched load, in the same way as the system presented in [26]. However, it requires the addition of a single *ADC* and the implementation of an arithmetic mean.

As regarding the computational complexity, it is linked to the procedure of averaging Q independent digital signals. In particular, if the digitised signal consists of K time samples of the total analog signal properly stored, then at the q-th step it is necessary to sum the K samples of the total signal associated with the realisation of the current thinned array factor with the K samples related to the partial sum of the previous $q-1$ thinned array factors. Consequently, the total number of operations consists of $(Q-1)\times K$ sums and a division by a constant. Therefore, the computational complexity does not depend on the number of sensors, but it is rather related to the number of samples taken at each acquisition and the number of acquisitions.

Finally, the system under discussion is adaptive in the sense as described in [1], since it could also be exploited for interference suppression. The related advantage, however, is that, depending on the environmental operating conditions, it can modulate both the number of acquisitions as well as the expected values of the coefficients $\{F_n^{(q)}\}_{n=1}^N$, for each q, to obtain better performance in terms of peak sidelobe level and/or of discrepancy between the actual and desired array factor. It can work in real-time, if cost admitting, but also in asynchronous mode in the case that the characteristics of the domain under investigation negligibly change during the Q acquisitions.

V. DISTANCE BETWEEN THE ACTUAL ARRAY FACTOR AND THE REFERENCE ONE AND LEVEL SURFACES FOR THE ACTUAL POWER PATTERN

In this section, some expressions are provided to characterise the discrepancy (*distance*) existing between the actual array factor and the reference array factor. In addition, level surfaces for the actual power pattern are also treated. The methodology presented here refers to the results discussed in [40], [42].

Let us suppose that the following random error function represents the distance, at the generic point (u,v), between the actual array factor and the reference one:

$$\begin{aligned} \varepsilon(u,v) &= \frac{|F_{ed}(u,v)-\mu(u,v)|^2}{|\mu(u,v)|^2} \\ &= \frac{\left[F_{ed_{\mathcal{R}}}(u,v)-\mu_{\mathcal{R}}(u,v)\right]^2+\left[F_{ed_{\mathcal{I}}}(u,v)-\mu_{\mathcal{I}}(u,v)\right]^2}{|\mu(u,v)|^2} \end{aligned} \quad (14)$$

where $\mu_{\mathcal{R}}(u,v)$ and $\mu_{\mathcal{I}}(u,v)$ represent the real and the imaginary parts of $\mu(u,v)=F_{ref}(u,v)$, respectively. The mean of

the above function represents a sort of relative mean squared error between $F_{ed}(u,v)$ and $\mu(u,v)$, namely:

$$\mu_\varepsilon(u,v) = E[\varepsilon(u,v)] = \frac{E\left[|F_{ed}(u,v)-\mu(u,v)|^2\right]}{|\mu(u,v)|^2} = \frac{E\left[|F_{ed}(u,v)|^2\right]-|\mu(u,v)|^2}{|\mu(u,v)|^2} = \frac{\sigma^2}{Q\,|\mu(u,v)|^2} \quad (15)$$

As regards to the variance of $\varepsilon(u,v)$, by exploiting the results shown in [40] it can be written that (with (u,v) implied):

$$\sigma_\varepsilon^2 = E\left[\varepsilon^2\right]-\mu_\varepsilon^2 = \frac{E\left[\left(F_{ed_\mathcal{R}}-\mu_\mathcal{R}\right)^4\right]}{|\mu|^4}+\frac{E\left[\left(F_{ed_\mathcal{I}}-\mu_\mathcal{I}\right)^4\right]}{|\mu|^4} + \frac{2E\left[\left(F_{ed_\mathcal{R}}-\mu_\mathcal{R}\right)^2\left(F_{ed_\mathcal{I}}-\mu_\mathcal{I}\right)^2\right]}{|\mu|^4}-\mu_\varepsilon^2 \quad (16)$$

The computation of the $\sigma_\varepsilon^2(u,v)$ turns out to be somewhat tedious in the general case, *i.e.*, when $F_{ed_\mathcal{R}}(u,v)$ and $F_{ed_\mathcal{I}}(u,v)$ have a generic probability joint distribution at (u,v). However, since the problem under consideration is such that the number of antenna elements is high enough to invoke the Lyapunov central limit theorem [2], such random functions can be assumed to be jointly Gaussian. In this case, by exploiting (15), the higher order central moments of a Gaussian random variable and the Isserlis theorem [47], it can be written that (with (u,v) implied):

$$\sigma_\varepsilon^2 = \frac{3\sigma_\mathcal{R}^4+3\sigma_\mathcal{I}^4+2\sigma_\mathcal{R}^2\sigma_\mathcal{I}^2+4\,\mathcal{K}^2-\left(\sigma^2/Q\right)^2}{|\mu|^4} \quad (17)$$

where $\mathcal{K}(u,v)$ is the covariance between $F_{ed_\mathcal{R}}(u,v)$ and $F_{ed_\mathcal{I}}(u,v)$, respectively (see the Appendix). At this point, as in [40], it is possible to exploit Cantelli's inequality to obtain a lower bound for the probability distribution of $\varepsilon(u,v)$ (with ξ being a positive real number):

$$\mathcal{P}_r\{\varepsilon(u,v)\le\mu_\varepsilon(u,v)+\xi\}\ge 1-\frac{\sigma_\varepsilon^2(u,v)}{\sigma_\varepsilon^2(u,v)+\xi^2} \quad (18)$$

Referring to the results in [42], it turns out to be advantageous to address the characterisation of the power pattern by exploiting the following relationships (with $\eta\in[0,100]$):

$$\begin{cases} r_\eta(u,v)\ge E[P_{ed}(u,v)]-\sigma_{P_{ed}}(u,v)\sqrt{\frac{1-\eta\%}{\eta\%}} \\ r_\eta(u,v)\le E[P_{ed}(u,v)]+\sigma_{P_{ed}}(u,v)\sqrt{\frac{\eta\%}{1-\eta\%}} \end{cases} \quad (19)$$

where $r_\eta(u,v)$ is the $\eta\%$ level surface for the actual power pattern, *i.e.*, $\mathcal{P}_r\{P_{ed}(u,v)\le r_\eta(u,v)\}=\eta\%$, while $\sigma_{P_{ed}}^2(u,v)$ is the variance of $P_{ed}(u,v)$, given by [40]:

$$\sigma_{P_{ed}}^2 = 4\left(\mu_\mathcal{R}^2\sigma_\mathcal{R}^2+\mu_\mathcal{I}^2\sigma_\mathcal{I}^2+\mathcal{K}^2+2\mathcal{K}\mu_\mathcal{R}\mu_\mathcal{I}\right) + 2\left(\sigma_\mathcal{R}^4+\sigma_\mathcal{I}^4\right) \quad (20)$$

Other results presented in [40] and [42] can be exploited to the study of the distribution of $P_{ed}(u,v)$. However, in order not to overburden the discussion and since this is not the main objective of the present work, the interested reader is referred to the above references for a more in-depth characterisation of the actual power pattern.

VI. NUMERICAL RESULTS

In this section, some numerical results are shown to validate the proposed sensing system. To this end, the excitation coefficients of the various reference arrays are obtained by sampling the Hansen *continuous* circular source for low peak sidelobe-level design [49]. All reference arrays are represented by periodic square grid arrays with half a wavelength uniformly spaced elements, as in [25], where the only elements within the circle included in the square grid are retained. The results are presented along array factor cuts, and the independent observation variables are represented as follows:

$$\begin{cases} u=\rho\,\cos\gamma \\ v=\rho\,\sin\gamma \end{cases} \quad (21)$$

with $\rho\in[0,2]$ and $\gamma\in[0,2\pi]$. Evaluating both $F_{ed}(\rho,\gamma)$ and $F_{ed}(-\rho,\gamma)$, with γ fixed and for $\rho\in[0,2]$, the behaviour of the array factor is determined along the diameter of the full scan-range which forms the angle γ with the u-axis. However, since $F_{ed}(u,v)$ is a Hermitian function, then it is sufficient to consider the values of γ belonging to the interval $(-\pi/2,\pi/2)$, namely, to evaluate $F_{ed}(u,v)$ only in the portion of the full scan-range belonging to the first and the fourth quadrants of the $u-v$ plane. The array factor is sampled with a step equal to $\Delta\rho=1/(8Lx)$. As a result, along the u-axis ($\gamma=0$) and the v-axis ($\gamma=\pi/2$), the sampling rate is four times higher than the Nyquist rate related to the power-pattern.

Fig. 2(a) shows the configuration of the array whose feeding network is equipped with the circuitry necessary to implement the excitation diversity. Each blue circle represents a radiator that can be dynamically turned on and off during the sensing process. Figure 2(b) shows the values of the excitation coefficients of the reference array, *i.e.*, the coefficients $\{A_n\}_{n=1}^N$, obtained by sampling the Hansen reference current distribution. The parameter of the Hansen design is equal to $H=1.72535$, so to obtain a reference array factor with a peak sidelobe-level equal to -40 dB. Fig. 3 compares the normalised magnitude of the reference array factor, the normalised magnitude of a realisation of a thinned array factor, and the realisations of the normalised magnitude of array factors related to thinned arrays with excitation diversity. The diagrams relate to three cuts of the aforementioned array factors, for $\gamma\in\{0,\pi/4,\pi/2\}$. In particular, two configurations of thinned arrays implementing excitation diversity are considered, the first performing 30 acquisitions while the second 50 acquisitions. As it can be seen, if considering more acquisitions, an improvement in terms of peak sidelobe-level can be achieved. In fact, going from a single (classic version of thinned array) to

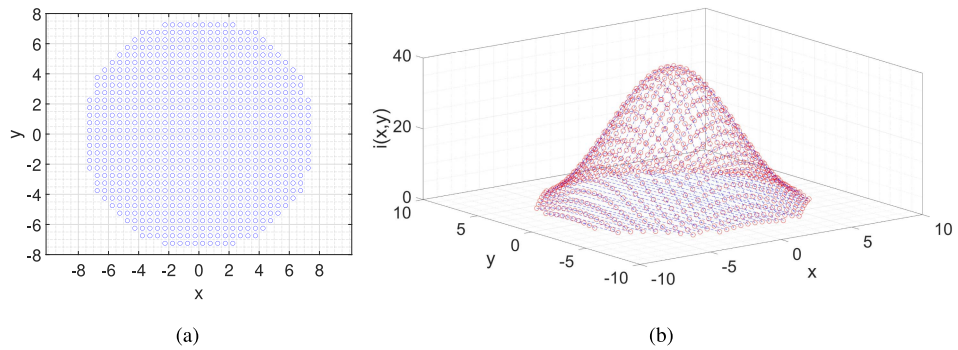

FIGURE 2. a) Thinned array configuration with excitation diversity; b) Reference current distribution resulting from the sampling of the Hansen continuous source associated with a peak sidelobe-level of −40 dB. The variables *x* and *y* are expressed in wavelengths.

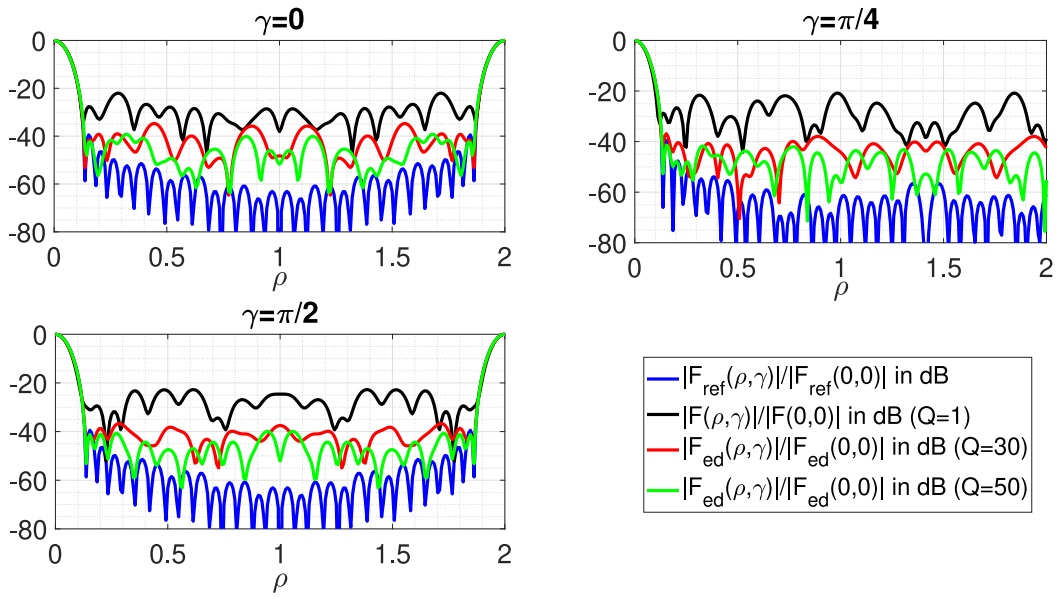

FIGURE 3. Comparison, for different cuts, between the magnitude of the reference array factor, a realisation of the array factor magnitude of a (standard) statistically thinned array ($Q = 1$) and the realisations of the array factor magnitudes of statistically thinned arrays with excitation diversity (for $Q = 30$ and $Q = 50$). All functions are normalised to their maximum value. The reference current is given by the Hansen design for circular apertures with a peak sidelobe level of −40 dB. The nominal number of elements is $N = 1024$ and $\alpha = 1$ (natural thinning).

more acquisitions, the reduction of the peak sidelobe-level can be considerable. Indeed, referring to the cut for $\gamma = 0$, it can be noted that the black curve (classic array thinning) almost reaches −20 dB, while the red curve, which relates to 30 acquisitions, does not exceed −35 dB. However, the green curve, related to 50 acquisitions, does not exceed the value of −40 dB. Therefore, it is clearly evident the improvement achievable from the implementation of excitation diversity in thinned arrays to obtain higher quality received signals.

It is worth noting that the green curves, related to the case of 50 acquisitions, have a lower mean value than the red curves corresponding to the case of 30 acquisitions. Obviously, for $Q \to \infty$, the actual array factor gets closer and closer to the desired one, as the term σ^2/Q tends to zero. In this regard, only for conceptual purposes, Fig. 4 shows the comparison between the desired pattern and that obtained after the acquisitions and the subsequent sample mean operation of 2000 realisations of the thinned array factor. As it can be seen, the various cuts of the thinned array factor, obtained from the aforementioned acquisitions, are very close to those associated with the desired array factor.

Fig. 5 shows the three-dimensional comparison between the array factors related to the results of the previous figures. To obtain these figures, the sampling step has been set equal to $\Delta_\rho = 1/(2L_x)$. The 3D images show the realisations of $|F_{ed}(u, v)|$ in the domain $[-2, 2] \times [-2, 2]$, for $Q = 1, 30, 50$. This domain encompasses the full-scan range, as the latter is a circular region with a radius equal to 2. However, any grating-lobes that may enter the visible space can be noted, which are positioned at points $(u, v) = \{(2, 0), (0, 2), (-2, 0), (0, -2)\}$. It can be noted that the excitation diversity allows

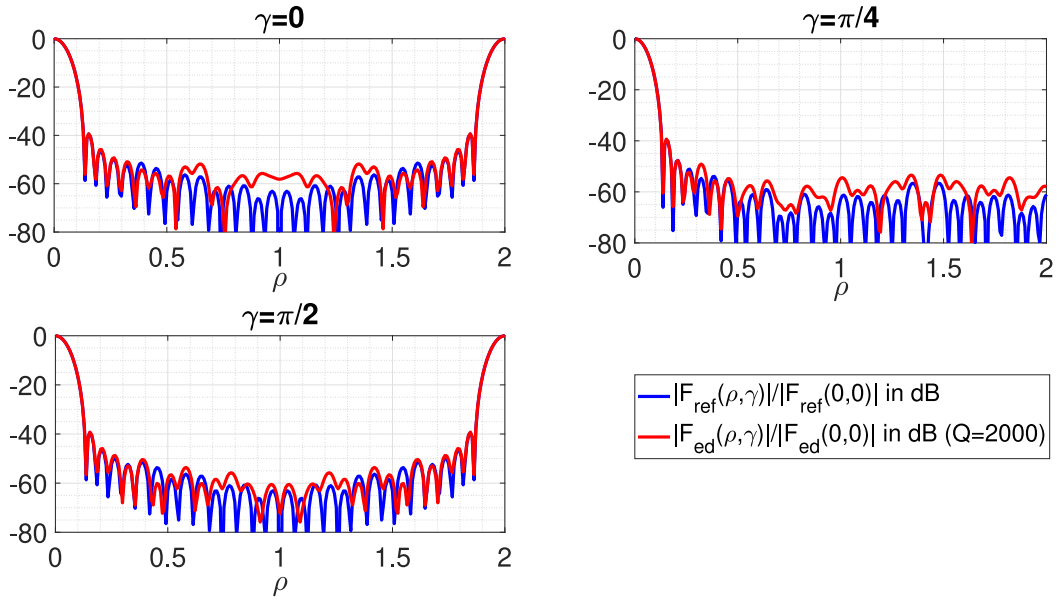

FIGURE 4. Comparison, for different cuts, between the magnitude of the reference array factor and the realisation of the array factor magnitude of the statistically thinned array with excitation diversity (for $Q = 2000$). Both functions are normalised to their maximum value. The reference current is given by the Hansen design for circular apertures with a peak sidelobe level of −40 dB. The nominal number of elements is $N = 1024$ and $\alpha = 1$ (natural thinning).

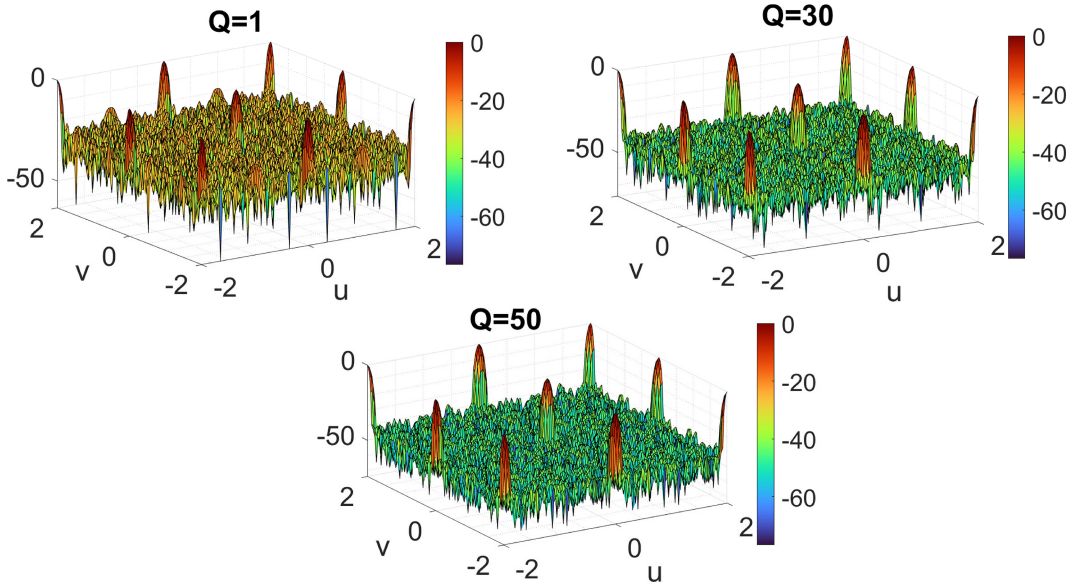

FIGURE 5. 3D view of a normalised array factor magnitude realisation of a classic thinned array ($Q = 1$), a normalised array factor magnitude realisation of a thinned array with excitation diversity implementing 30 acquisitions ($Q = 30$), and a realisation of the normalised array factor magnitude of a thinned array with excitation diversity implementing 50 acquisitions ($Q = 50$).

not only to obtain a performance improvement in the principal plane, but also in the remaining part of the full scan-range.

Now, in order to further enforce the validation of the proposed method, let us consider a structure for the array factor similar to that proposed in [39], *i.e.*, modelling simultaneous multiple beams. To do this, the spectral observation variables are redefined as $u = \sin\theta\,\cos\phi$ and $v = \sin\theta\,\sin\phi$. In this case, the full-scan range coincides with the visible space, *i.e.*, with a circularly-bounded region having a radius equal to 1 and centred at $(u, v) = (0, 0)$. Fig. 6 compares the normalised magnitude of the reference array factor, the normalised magnitude of a realisation of a thinned array factor, and the realisations of the normalised magnitude of array factors related to thinned arrays with excitation diversity. The diagrams relate to three cuts of the aforementioned array factors, for $v = 0$, $u = v$ and $u = 0$. Also in this case, considering more acquisitions allows to obtain an improvement in terms of peak sidelobe-level. Then, in order to get a more general view, Fig. 7 compares the 3D view of array factors related to the previous figure, showing, in this case, the normalised realisations of $|F_{ed}(u, v)|$ in the domain

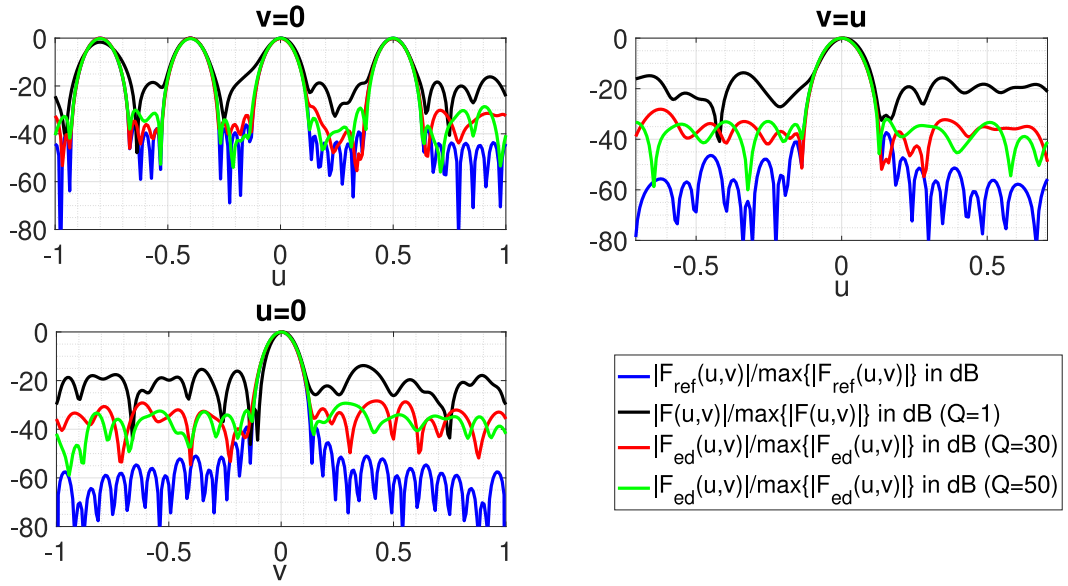

FIGURE 6. Comparison, for different cuts, between the magnitude of the reference array factor, a realisation of the array factor magnitude of a (standard) statistically thinned array ($Q = 1$) and the realisations of the array factor magnitudes of statistically thinned arrays with excitation diversity (for $Q = 30$ and $Q = 50$). All functions are normalised to their maximum value. The reference current is given by the Hansen design for circular apertures with a peak sidelobe level of -40 dB, and the phases of the excitation coefficients are such as to have multiple simultaneous beams along the cut $v = 0$. The nominal number of elements is $N = 1024$ and $\alpha = 1$ (natural thinning).

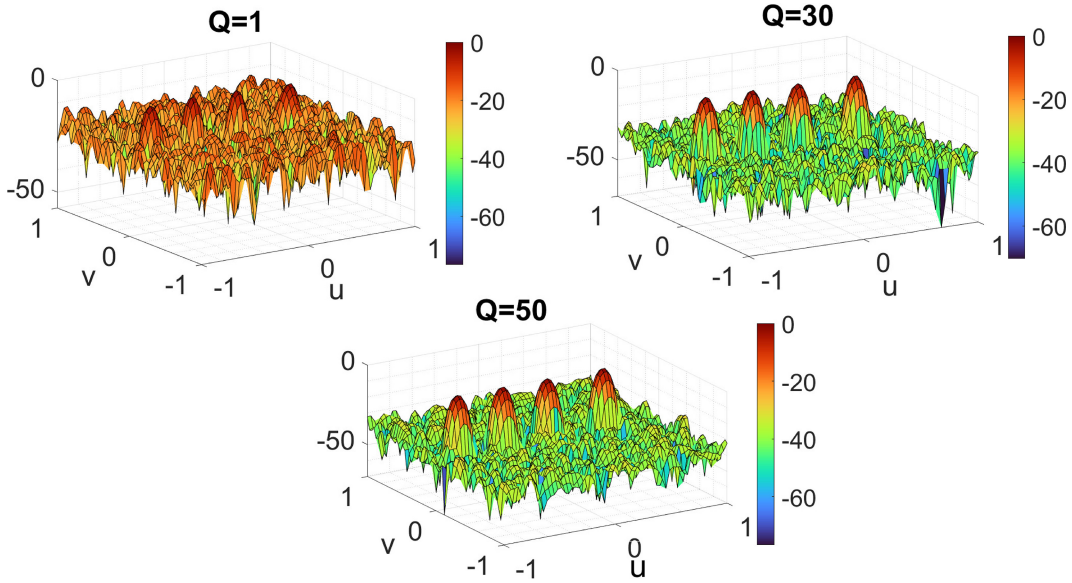

FIGURE 7. 3D view of a normalised array factor magnitude realisation of a classic thinned array ($Q = 1$), a normalised array factor magnitude realisation of a thinned array with excitation diversity implementing 30 acquisitions ($Q = 30$), and a realisation of the normalised array factor magnitude of a thinned array with excitation diversity implementing 50 acquisitions ($Q = 50$). The reference current is given by the Hansen design for circular apertures with a peak sidelobe level of -40 dB, and the phases of the excitation coefficients are such as to have multiple simultaneous beams along the cut $v = 0$.

$[-1, 1] \times [-1, 1]$, for $Q = 1$, 30, 50. Again, a significant improvement can be observed, due to the implementation of the excitation diversity methodology.

Table 1 shows the computation time of the 3D array factor magnitudes as a function of the number of acquisitions in the case of multiple beams. The adopted computer is a laptop with an Intel core I7 processor (frequency 2.80 GHz, quad-core, 16 GB RAM).

Finally, to consider a more realistic scenario, in Fig. 8 the results referred to the principal planes of an array having the same geometry of the array in Fig. 2(a) are presented. The assumed antenna elements are given by half-wavelength dipole antennas, placed in the $x-y$ plane and oriented along

TABLE 1. Computation time for the 3D array factor magnitudes as a function of the number of acquisitions in the multibeam case.

Number of acquisition (Q)	Computation time [s]
1	0.0541
30	0.4095
50	0.6021

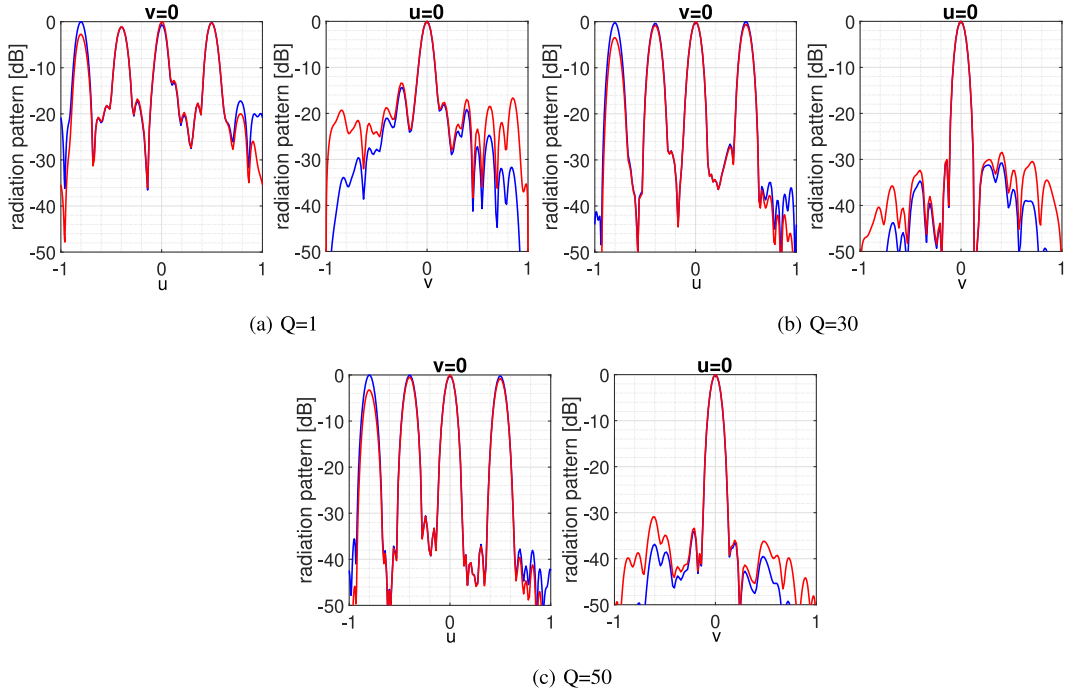

FIGURE 8. Comparison between the theoretical array pattern with neglected mutual couplings (blue lines) and that based on the embedded element pattern method (red lines) - planar array of half-wavelength dipole antennas, in the principal planes of the array ($\phi = 0° \Rightarrow v = 0$ and $\phi = 90° \Rightarrow u = 0$). The reference pattern has four beams.

the y axis. The results are relative to the four-beams case. The theoretical patterns (blue lines) are obtained by assuming the absence of mutual coupling, and thus computing the radiation pattern as the product of the array factor with the isolated element pattern of a half-wavelength dipole antenna. The red lines, on the other hand, are obtained by using the embedded element pattern method [1], [50], leading to accurately take into account the mutual couplings in large arrays. In this case, the array pattern is obtained by multiplying the array factor with the embedded element pattern of one of the most central elements of the array, which is determined by exploiting CST Studio Suite [51]. As it can be seen, no significant effect on the pattern is given in this case by mutual couplings. Instead, this example confirms that, as the acquisitions increase, the level of the secondary lobes tends to decrease.

VII. CONCLUSION

In this work, a design scheme for thinned arrays incorporating excitation diversity has been introduced. The presented approach provides significant potential advantages to improve the quality of the received signals. Indeed, it has been demonstrated that the sample mean of different sample paths of the stochastic thinned array factor allows for significantly improved performance in reducing the peak sidelobe-level, as well as the discrepancy between the actual array factor and the desired one. Indeed, the statistical mean of the squared magnitude of the array factor consists of the sum of the desired power-pattern and a term representing the variance of the array factor. Therefore, with the proposed excitation diversity approach, easily implementable through the adoption of proper switches, it is possible to advantageously control the above variance by suitably setting the number of acquisitions. This approach can be successfully adopted in multiple microwave sensing contexts.

APPENDIX A
NOMENCLATURE

$F_{ref}(u, v) \rightarrow$	reference array factor
$F(u, v) \rightarrow$	array factor of a classic thinned array
$\mu(u, v) \rightarrow$	expected value of $F(u, v)$
$\sigma^2 \rightarrow$	variance of $F(u, v)$
$\mu_P(u, v) \rightarrow$	expected value of $\lvert F(u, v)\rvert^2$
$F_{ed}(u, v) \rightarrow$	equivalent actual array factor of the thinned array with excitation diversity
$F_q(u, v) \rightarrow$	array factor of the thinned array related to the q-th acquisition, which is independent of all other thinned array factors $F_l(u, v)$, with $l \neq q$
$F_{ed_{\mathcal{R}}}(u, v) \rightarrow$	real part of $F_{ed}(u, v)$
$F_{ed_{\mathcal{I}}}(u, v) \rightarrow$	imaginary part of $F_{ed}(u, v)$
$F_{q_{\mathcal{R}}}(u, v) \rightarrow$	real part of $F_q(u, v)$
$F_{q_{\mathcal{I}}}(u, v) \rightarrow$	imaginary part of $F_q(u, v)$
$F_n^{(q)} \rightarrow$	binary random magnitude of the excitation coefficient of the n-th sensor associated with the q-th acquisition

$\mu_{ed}(u,v) \rightarrow$ expected value of $F_{ed}(u,v)$, coinciding with $\mu(u,v)$
$E[P_{ed}(u,v)] \rightarrow$ expected value of $|F_{ed}(u,v)|^2$
$\sigma^2_{P_{ed}}(u,v) \rightarrow$ variance of $|F_{ed}(u,v)|^2$
$\mu_{\mathcal{R}}(u,v) \rightarrow$ expected value of both $F_{ed_{\mathcal{R}}}(u,v)$ and $F_{q_{\mathcal{R}}}(u,v)$
$\mu_{\mathcal{I}}(u,v) \rightarrow$ expected value of both $F_{ed_{\mathcal{I}}}(u,v)$ and $F_{q_{\mathcal{I}}}(u,v)$
$\sigma^2_{\mathcal{R}}(u,v) \rightarrow$ variance of $F_{ed_{\mathcal{R}}}(u,v)$
$\sigma^2_{\mathcal{I}}(u,v) \rightarrow$ variance of $F_{ed_{\mathcal{I}}}(u,v)$
$Q \times \sigma^2_{\mathcal{R}}(u,v) \rightarrow$ variance of $F_{q_{\mathcal{R}}}(u,v)$
$Q \times \sigma^2_{\mathcal{I}}(u,v) \rightarrow$ variance of $F_{q_{\mathcal{I}}}(u,v)$
$\varepsilon(u,v) \rightarrow$ discrepancy (distance) between $F_{ed}(u,v)$ and $F_{ref}(u,v)$
$\mu_{\varepsilon}(u,v) \rightarrow$ expected value of $\varepsilon(u,v)$
$\sigma^2_{\varepsilon}(u,v) \rightarrow$ variance of $\varepsilon(u,v)$

APPENDIX B
SQUARED MAGNITUDE OF $F_{REF}(U,V)$, MOMENTS OF $F_Q(U,V)$ AND MOMENTS AND COVARIANCE OF $F_{ED_{\mathcal{R}}}(U,V)$ AND $F_{ED_{\mathcal{I}}}(U,V)$

The squared magnitude of the reference array factor is:

$$|F_{ref}(u,v)|^2 = \sum_{n=1}^{N}\sum_{m=1}^{N} A_n A_m\, e^{j2\pi\left[(x_n-x_m)u+(y_n-y_m)v\right]}$$
$$= \sum_{n=1}^{N} A_n^2 + \sum_{n=1}^{N}\sum_{m=1,m\neq n}^{N} A_n A_m\, e^{j2\pi\left[(x_n-x_m)u+(y_n-y_m)v\right]} \quad (22)$$

Taking into account that $E[F_n^{(q)}] = E[F_n^{(h)}] = \alpha A_n / \max\{A_n\}_{n=1}^N$ and that $E[\{F_n^{(q)}\}^2] = E[\{F_n^{(h)}\}^2] = E[F_n^{(q)}]$ for any value of q and h, the mean and the mean squared magnitude of the generic $F_q(u,v)$ can be computed as follows:

$$E\left[F_q(u,v)\right] = C\sum_{n=1}^{N} E\left[F_n^{(q)}\right] e^{j2\pi(x_n u+y_n v)}$$
$$= \frac{\max\{A_n\}_{n=1}^N}{\alpha}\sum_{n=1}^{N}\frac{\alpha A_n}{\max\{A_n\}_{n=1}^N} e^{j2\pi(x_n u+y_n v)}$$
$$= \sum_{n=1}^{N} A_n\, e^{j2\pi(x_n u+y_n v)}$$
$$= \mu(u,v) = F_{ref}(u,v) \quad (23)$$
$$= C^2\sum_{n=1}^{N} E\left[F_n^{(q)}F_m^{(q)}\right] e^{j2\pi\left[(x_n-x_m)u+(y_n-y_m)v\right]}$$
$$= C^2\sum_{n=1}^{N} E\left[F_n^{(q)}\right] + C^2\sum_{n=1}^{N}\sum_{m=1,m\neq n}^{N}\left\{E\left[F_n^{(q)}\right]E\left[F_m^{(q)}\right]\right.$$
$$\left.\times\, e^{j2\pi\left[(x_n-x_m)u+(y_n-y_m)v\right]}\right\}$$
$$= \frac{\max\{A_n\}_{n=1}^N}{\alpha}\sum_{n=1}^{N} A_n + \sum_{n=1}^{N}\sum_{m=1,m\neq n}^{N}\left\{A_n A_m\right.$$
$$\left.\times\, e^{j2\pi\left[(x_n-x_m)u+(y_n-y_m)v\right]}\right\} = \mu_P(u,v) \quad (24)$$

The variance of the real part of $F_{ed}(u,v)$ is given as:

$$\sigma^2_{\mathcal{R}}(u,v) = E\left[F^2_{ed_{\mathcal{R}}}(u,v)\right] - \mu^2_{\mathcal{R}}(u,v)$$
$$= \frac{C^2}{Q}\sum_{n=1}^{N} p_n(1-p_n)\cos^2\left[2\pi(x_n u+y_n v)\right] \quad (25)$$

The variance of the imaginary part of $F_{ed}(u,v)$ can be written as:

$$\sigma^2_{\mathcal{I}}(u,v) = E\left[F^2_{ed_{\mathcal{I}}}(u,v)\right] - \mu^2_{\mathcal{I}}(u,v)$$
$$= \frac{C^2}{Q}\sum_{n=1}^{N} p_n(1-p_n)\sin^2\left[2\pi(x_n u+y_n v)\right] \quad (26)$$

and it is easy to prove that $\sigma^2/Q = \sigma^2_{\mathcal{R}}(u,v) + \sigma^2_{\mathcal{I}}(u,v)$. Furthermore, it is also easy to prove that $Q\times\sigma^2_{\mathcal{R}}(u,v)$ is the variance of the real part of the generic $F_q(u,v)$, and $Q\times\sigma^2_{\mathcal{I}}(u,v)$ is the variance of the imaginary part of the generic $F_q(u,v)$, since for $Q=1$, $F_{ed}(u,v)$ coincides with the classic thinned array factor $F(u,v)$, that, at the generic point (u,v), is identically distributed as the generic $F_q(u,v)$. Finally, the covariance function between the real and imaginary parts of $F_{ed}(u,v)$ is given as:

$$\mathcal{K}(u,v) = E\left[F_{ed_{\mathcal{R}}}(u,v)F_{ed_{\mathcal{I}}}(u,v)\right] - \mu_{\mathcal{R}}(u,v)\mu_{\mathcal{I}}(u,v)$$
$$= \frac{C^2}{Q}\sum_{n=1}^{N} p_n(1-p_n)\cos\left[2\pi(x_n u+y_n v)\right]\sin\left[2\pi(x_n u+y_n v)\right]. \quad (27)$$

REFERENCES

[1] R. L. Haupt, *Antenna Arrays: A Computational Approach*. Hoboken, NJ, USA: Wiley, 2010.
[2] Y. T. Lo, "A mathematical theory of antenna arrays with randomly spaced elements," *IEEE Trans. Antennas Propag.*, vol. 12, no. 3, pp. 257–268, May 1964. doi: 10.1109/TAP.1964.1138220.
[3] A.Ishimaru and Y.-S. Chen, "Thinning and broadbanding antenna arrays by unequal spacings," *IEEE Trans. Antennas Propag.*, vol. 13, no. 1, pp. 34–42, Jan. 1965, doi: 10.1109/TAP.1965.1138378.
[4] B. D. Steinberg, "The peak sidelobe of the phased array having randomly located elements," *IEEE Trans. Antennas Propag.*, vol. 20, no. 2, pp. 129–136, Mar. 1972, doi: 10.1109/TAP.1972.1140162.
[5] G. Buonanno and R. Solimene, "Comparing different schemes for random arrays," *Prog. Electromagn. Res. B*, vol. 71, pp. 107–118, Nov. 2016. doi: 10.2528/PIERB16081001.
[6] R. J. Mailloux, *Phased Array Antenna Handbook* (Artech House Antennas and Propagation Library), 2nd ed. Norwood, MA, USA: Artech House, 2005.
[7] F. Venneri, S. Costanzo, G. Di Massa, A. Borgia, P. Corsonello, and M. Salzano, "Design of a reconfigurable reflectarray based on a varactor tuned element," in *Proc. 6th Eur. Conf. Antennas Propag. (EUCAP)*, Mar. 2012, pp. 2628–2631, doi: 10.1109/EuCAP.2012.6206624.
[8] S. Costanzo, F. Venneri, G. Di Massa, and G. Angiulli, "Synthesis of microstrip reflectarrays as planar scatterers for SAR interferometry," *Electron. Lett.*, vol. 33, no. 3, pp. 266–267, 2003, doi: 10.1049/el:20030201.

[9] S. D. Assimonis, T. V. Yioultsis, and C. S. Antonopoulos, "Design and optimization of uniplanar EBG structures for low profile antenna applications and mutual coupling reduction," *IEEE Trans. Antennas Propag.*, vol. 60, no. 10, pp. 4944–4949, Oct. 2012, doi: 10.1109/TAP.2012.2210178.

[10] K. Wei, J.-Y. Li, L. Wang, Z.-J. Xing, and R. Xu, "Mutual coupling reduction by novel fractal defected ground structure bandgap filter," *IEEE Trans. Antennas Propag.*, vol. 64, no. 10, pp. 4328–4335, Oct. 2016, doi: 10.1109/TAP.2016.2591058.

[11] S. Ghosh, T.-N. Tran, and T. Le-Ngoc, "Dual-layer EBG-based miniaturized multi-element antenna for MIMO systems," *IEEE Trans. Antennas Propag.*, vol. 62, no. 8, pp. 3985–3997, Aug. 2014, doi: 10.1109/TAP.2014.2323410.

[12] R. Anitha, V. P. Sarin, P. Mohanan, and K. Vasudevan, "Enhanced isolation with defected ground structure in MIMO antenna," *Electron. Lett.*, vol. 50, no. 24, pp. 1784–1786, 2014, doi: 10.1049/el.2014.2795.

[13] A. Kumar, J. Mohan, and H. Gupta, "Surface wave suppression of microstrip antenna using different EBG designs," in *Proc. Int. Conf. Signal Process. Commun.* (ICSC), Mar. 2015, pp. 355–359, doi: 10.1109/ICSPCom.2015.7150676.

[14] R. L. Haupt, "Thinned arrays using genetic algorithms," *IEEE Trans. Antennas Propag.*, vol. 42, no. 7, pp. 993–999, Jul. 1994, doi: 10.1109/8.299602.

[15] V. Murino, A. Trucco, and C. Regazzoni, "Synthesis of unequally spaced arrays by simulated annealing," *IEEE Trans. Signal Process.*, vol. 44, no. 1, pp. 119–123, Jan. 1996, doi: 10.1109/78.482017.

[16] M. Khodier and C. G. Christodoulou, "Linear array geometry synthesis with minimum sidelobe level and null control using particle swarm optimization," *IEEE Trans. Antennas Propag.*, vol. 53, no. 8, pp. 2674–2679, Aug. 2005, doi: 10.1109/TAP.2005.851762.

[17] O. Quevedo-Teruel and E. Rajo-Iglesias, "Ant colony optimization in thinned array synthesis with minimum sidelobe level," *IEEE Antennas Wireless Propag. Lett.*, vol. 5, no. 1, pp. 349–352, Aug. 2006, doi: 10.1109/LAWP.2006.880693.

[18] S. K. Goudos and J. N. Sahalos, "Design of large thinned arrays using different biogeography-based optimization migration models," *Int. J. Antennas Propag.*, vol. 2016, Sep. 2016, Art. no. 5359298, doi: 10.1155/2016/5359298.

[19] F. Boulos et al., "A computational inversion method for interference suppression in reconfigurable thinned ring arrays," *J. Phys. Conf. Series*, vol. 1476, no. 1, 2020, Art. no. 12016, doi: 10.1088/1742-6596/1476/1/012016.

[20] E. Tohidi, M. M. Nayebi, and H. Behroozi, "Dynamic programming applied to large circular arrays thinning," *IEEE Trans. Antennas Propag.*, vol. 66, no. 8, pp. 4025–4033, Aug. 2018, doi: 10.1109/TAP.2018.2842258.

[21] W. P. M. N. Keizer, "Large planar array thinning using iterative FFT techniques," *IEEE Trans. Antennas Propag.*, vol. 57, no. 10, pp. 3359–3362, Oct. 2009, doi: 10.1109/TAP.2009.2029382.

[22] W. P. M. N. Keizer, "Synthesis of thinned planar circular and square arrays using density tapering," *IEEE Trans. Antennas Propag.*, vol. 62, no. 4, pp. 1555–1563, Apr. 2014, doi: 10.1109/TAP.2013.2267194.

[23] X.-K. Wang, Y.-C. Jiao, and Y.-Y. Tan, "Synthesis of large thinned planar arrays using a modified iterative Fourier technique," *IEEE Trans. Antennas Propag.*, vol. 62, no. 4, pp. 1564–1571, Apr. 2014, doi: 10.1109/TAP.2014.2302836.

[24] T. M. Maher and D. K. Cheng, "Random removal of radiators from large linear arrays," *IEEE Trans. Antennas Propag.*, vol. AP-11, no. 2, pp. 106–112, Mar. 1963, doi: 10.1109/TAP.1963.1138000.

[25] M. Skolnik, J. W. Sherman, III, and F. Ogg Jr., "Statistically designed density-tapered arrays," *IEEE Trans. Antennas Propag.*, vol. 12, no. 4, pp. 408–417, Jul. 1964, doi: 10.1109/TAP.1964.1138239.

[26] R. L. Haupt, "Adaptively thinned arrays," *IEEE Trans. Antennas Propag.*, vol. 63, no. 4, pp. 1626–1632, Apr. 2015, doi: 10.1109/TAP.2015.2394785.

[27] R. L. Haupt, "Adaptive low sidelobe thinning," *Proc. Int. Conf. Electromag. Adv. Appl.* (ICEAA), Sep. 2013, pp. 167–168, doi: 10.1109/ICEAA.2013.6632214.

[28] R. J. Mailloux and E. Cohen, "Statistically thinned arrays with quantized element weights," *IEEE Trans. Antennas Propag.*, vol. 39, no. 4, pp. 436–447, Apr. 1991, doi: 10.1109/8.81455.

[29] G. Buonanno and R. Solimene, "Global characterization of linear statistically thinned antenna arrays," *IEEE Access*, vol. 9, pp. 119629–119640, 2021, doi: 10.1109/ACCESS.2021.3107095.

[30] Y. T. Lo, "Random periodic arrays," *Radio Sci.*, vol. 3, no. 5, pp. 425–436, 1968, doi: 10.1002/rds196835425.

[31] G. Buonanno and R. Solimene, "Large linear random symmetric arrays," *Prog. Electromagn. Res. M*, vol. 52, pp. 67–77, Nov. 2016, doi: 10.2528/PIERM16062706.

[32] K. Buchanan and G. H. Huff, "A stochastic mathematical framework for the analysis of spherically-bound random arrays," *IEEE Trans. Antennas Propag.*, vol. 62, no. 6, pp. 3002–3011, Jun. 2014, doi: 10.1109/TAP.2014.2313142.

[33] G. Buonanno and R. Solimene, "Generalised random binned antenna arrays," *Progr. Electromagn. Res. C*, vol. 78, pp. 129–143, Oct. 2017, doi: 10.2528/PIERC17081806.

[34] G. Buonanno and R. Solimene, "Unequally-excited linear totally random antenna arrays for multi-beam patterns," *IET Microw. Antennas Propag.*, vol. 12, no. 10, pp. 1671–1678, 2018, doi: 10.1049/iet-map.2017.1206.

[35] A. G. Kanatas, "Analysis of planar random arrays with stochastic geometry tools," *IEEE Trans. Antennas Propag.*, vol. 70, no. 3, pp. 1906–1918, Mar. 2022, doi: 10.1109/TAP.2021.3113724.

[36] G. Buonanno and R. Solimene, "Unequally excited generalised random binned antenna arrays," *IET Microw. Antennas Propag.*, vol. 13, no. 14, pp. 2531–2538, 2019, doi: 10.1049/iet-map.2018.6094.

[37] K. Buchanan, M. Rodriguez, S. Wheeland, D. Overturf, O. Sternberg, and G. H. Huff, "Statistical analysis and discussion of circularly bound random antenna array distributions," *Proc. IEEE Int. Symp. Phased Array Syst. Technol.* (PAST), Oct. 2019, pp. 1–8, doi: 10.1109/PAST43306.2019.9020752.

[38] K. Buchanan et al., "Analysis of collaborative beamforming for circularly bound random antenna array distributions,," Nav. Inf. Warfare Center Pac. (NIWC Pacific), San Diego, CA, USA, Rep. 3218, Nov. 2020, doi: 10.13140/RG.2.2.16399.71848.

[39] G. Buonanno, S. Costanzo, and R. Solimene, "Statistically thinned array antennas for simultaneous multibeam applications," *IEEE Access*, vol. 10, pp. 60230–60240, Jun. 2022, doi: 10.1109/ACCESS.2022.3181168.

[40] G. Buonanno, S. Costanzo, and R. Solimene, "Broadband statistically designed thinned-binned array antennas," *IEEE Trans. Antennas Propag.*, vol. 71, no. 3, pp. 2454–2466, Mar. 2023, doi: 10.1109/TAP.2023.3236793.

[41] S. Costanzo, "Synthesis of multi-step coplanar waveguide-to-microstrip transition," *Progr. Electromagn. Res.*, vol. 113, pp. 111–126, Jan. 2011, doi: 10.2528/PIER10112908.

[42] G. Buonanno and S. Costanzo, "Fresnel-zone focused antenna arrays: Tolerance analysis for biomedical applications," *IEEE Trans. Antennas Propag.*, vol. 71, no. 3, pp. 7261–7272, Sep. 2023, doi: 10.1109/TAP.2023.3295493.

[43] B. Steinberg and E. Attia, "Sidelobe reduction of random arrays by element position and frequency diversity," *IEEE Trans. Antennas Propag.*, vol. 31, no. 6, pp. 922–930, Nov. 1983, doi: 10.1109/TAP.1983.1143175.

[44] C. A. Balanis and P. I. Ioannides, *Introduction to Smart Antennas*. San Rafael, CA, USA: Morgan & Claypool Publ., 2007.

[45] J. Pal, Y. Zhu, J. Lu, D. Dao, and F. Khan, "High power and reliable SPST/SP3T RF MEMS switches for wireless applications," *IEEE Electron Device Lett.*, vol. 37, no. 9, pp. 1219–1222, Sep. 2016, doi: 10.1109/LED.2016.2592539.

[46] S. Costanzo and G. Di Massa, "Direct far-field computation from bipolar near-field samples," *J. Electromagn. Waves Appl.*, vol. 20, no. 9, pp. 1137–1148, 2006, doi: 10.1163/156939306777442926.

[47] L. Isserlis, "On a formula for the product-moment coefficient of any order of a normal frequency distribution in any number of variables," *Biometrika*, vol. 12, nos. 1–2, pp. 134–139, 1918, doi: 10.1093/biomet/12.1-2.134.

[48] B. V. Gnedenko, *The Theory of Probability* (Translated from the Russian by George Yankovsky). Moscow, Russia: Mir Publ., 1978.

[49] R. Hansen, "A one-parameter circular aperture distribution with narrow beamwidth and low sidelobes," *IEEE Trans. Antennas Propag.*, vol. 24, no. 4, pp. 477–480, Jul. 1976, doi: 10.1109/TAP.1976.1141365.

[50] K. F. Warnick, D. B. Davidson, and D. Buck, "Embedded element pattern loading condition transformations for phased array modeling," *IEEE Trans. Antennas Propag.*, vol. 69, no. 3, pp. 1769–1774, Mar. 2021, doi: 10.1109/TAP.2020.3027593.

[51] (Dassault Systèmes, Vélizy-Villacoublay, France). *CST Studio Suite*. Accessed: Oct. 6, 2023. https://www.3ds.com/products-services/simulia/products/cst-studio-suite

SANDRA COSTANZO (Senior Member, IEEE) received the Laurea degree (summa cum laude) in computer engineering from the Università della Calabria, Italy, in 1996, and the Ph.D. degree in electronic engineering from the Università Mediterranea di Reggio Calabria, Italy, in 2000. In 2017, she awarded the Italian National Scientific Qualification for the Full Professor position. Since 2019, she has also been associate with IREA-CNR, Naples. She is currently an Associate Professor with the Università della Calabria, where she is the Coordinator of Master's Degree in Telecommunication Engineering and the Rector's Delegate for Health Safety. She teaches courses on electromagnetic waves propagation, antennas, remote sensing, radar, sensors, and electromagnetic diagnostics. She has authored or coauthored more than 200 contributions in international journals, books, and conferences. Her research interests are focused on near-field/far-field techniques, antenna measurement techniques, antenna analysis and synthesis, numerical methods in electromagnetics, millimeter-wave antennas, reflectarrays, synthesis methods for microwave structures, electromagnetic characterization of materials, biomedical applications, and radar technologies. She received the Telecom Prize for the Best Laurea Thesis in 1996, and the Best Academia and Research Application in Aerospace and Defense 2013 Award for the application of software-defined radar using the NI USRP 2920 platform. She is an Associate Editor of IEEE ACCESS, IEEE JOURNAL OF ELECTROMAGNETICS, RF AND MICROWAVES IN MEDICINE AND BIOLOGY, and *Electronics* (section "Microwave and Wireless Communications") and an Editorial Board Member of *Radioengineering* and *International Journal of RF and Microwave Computer-Aided Engineering*. She is an Editor of the books *Microwave Materials Characterization* (INTECH, 2012) and *Wave Propagation Concepts for Near-Future Telecommunication Systems* (INTECH, 2017). She was a Lead Editor of Special Issues titled: *Reflectarray Antennas: Analysis and Synthesis Techniques* in 2012, *Advances in Radar Technologies* in 2013, *Compressed Sensing: Applications in Radar and Communications* in 2016, *Bioengineering Applications of Electromagnetic Wave Propagation* in 2019, and *Microwave Sensors for Biomedical Applications* in 2020. She is a member of the IEEE MTT-28 Biological Effects and Medical Applications Committee, IEEE South Italy Geoscience and Remote Sensing Chapter, Consorzio Nazionale Interuniversitario per le Telecomunicazioni, Società Italiana di Elettromagnetismo, and Centro Interuniversitario sulle Interazioni fra Campi Elettromagnetici e Biosistemi and a Board Member of the IEEE AP/ED/MTT North Italy Chapter.

GIOVANNI BUONANNO (Member, IEEE) received the M.S. degree (summa cum laude) in electronic engineering from the Seconda Università degli Studi di Napoli (SUN), Aversa, Italy, in 2014, and the Ph.D. degree in industrial and information engineering from the University of Campania in 2018, defending his thesis in January 2019. In 2014, he joined the Research Group in Applied Electromagnetics, SUN. He is currently a Researcher with the University of Calabria. His research interests include nonuniformly spaced random arrays, biomedical signal processing, machine learning in electromagnetics, and tolerance analysis of antenna arrays.

Open Access funding provided by 'Università della Calabria' within the CRUI CARE Agreement